

Low-damage interface enhancement-mode AlN/GaN high electron mobility transistors with 41.6% PAE at 30 GHz

Si-Yu Liu(刘思雨), Jie-Jie Zhu(祝杰杰), Jing-Shu Guo(郭静姝), Kai Cheng(程凯), Min-Han Mi(宓珉瀚), Ling-Jie Qin(秦灵洁), Bo-Wen Zhang(张博文), Min Tang(唐旻), and Xiao-Hua Ma(马晓华)
Citation: Chin. Phys. B, 2023, 32 (**11**): 117302. DOI: 10.1088/1674-1056/acd8a5
Journal homepage: http://cpb.iphy.ac.cn; http://iopscience.iop.org/cpb

What follows is a list of articles you may be interested in

Chiral current regulation and detection of Berry phase in triangular triple quantum dots

Yue Qi(齐月), Yi-Ming Liu(刘一铭), Yuan-Dong Wang(王援东), Jian-Hua Wei(魏建华), and Zhen-Gang Zhu(朱振刚)
Chin. Phys. B, 2023, 32 (**8**): 087304. DOI: 10.1088/1674-1056/acd36c

Coherent manipulation of a tunable hybrid qubit via microwave control

Si-Si Gu(顾思思), Bao-Chuan Wang(王保传), Hai-Ou Li(李海欧), Gang Cao(曹刚), and Guo-Ping Guo(郭国平)
Chin. Phys. B, 2023, 32 (**8**): 087302. DOI: 10.1088/1674-1056/acd0a7

Research on self-supporting T-shaped gate structure of GaN-based HEMT devices

Peng Zhang(张鹏), Miao Li(李苗), Jun-Wen Chen(陈俊文), Jia-Zhi Liu(刘加志), and Xiao-Hua Ma(马晓华)
Chin. Phys. B, 2023, 32 (**6**): 067305. DOI: 10.1088/1674-1056/acaa27

Conductive path and local oxygen-vacancy dynamics: Case study of crosshatched oxides

Z W Liang(梁正伟), P Wu(吴平), L C Wang(王利晨), B G Shen(沈保根), and Zhi-Hong Wang(王志宏)
Chin. Phys. B, 2023, 32 (**4**): 047303. DOI: 10.1088/1674-1056/acb421

Low-resistance ohmic contacts on InAlN/GaN heterostructures with MOCVD-regrown n^+-InGaN and mask-free regrowth process

Jingshu Guo(郭静姝), Jiejie Zhu(祝杰杰), Siyu Liu(刘思雨), Jielong Liu(刘捷龙), Jiahao Xu(徐佳豪), Weiwei Chen(陈伟伟), Yuwei Zhou(周雨威), Xu Zhao(赵旭), Minhan Mi(宓珉瀚), Mei Yang(杨眉), Xiaohua Ma(马晓华), and Yue Hao(郝跃)
Chin. Phys. B, 2023, 32 (**3**): 037303. DOI: 10.1088/1674-1056/ac891b

---

Low-damage interface enhancement-mode AlN/GaN high electron mobility transistors with 41.6% PAE at 30 GHz

Si-Yu Liu(刘思雨)[1], Jie-Jie Zhu(祝杰杰)[1,†], Jing-Shu Guo(郭静姝)[1], Kai Cheng(程凯)[2], Min-Han Mi(宓珉瀚)[1], Ling-Jie Qin(秦灵洁)[1], Bo-Wen Zhang(张博文)[1], Min Tang(唐旻)[3], and Xiao-Hua Ma(马晓华)[1,‡]

[1] *Key Laboratory of Wide Bandgap Semiconductor Technology, School of Microelectronics, Xidian University, Xi'an* 710071, *China*
[2] *Enkris Semiconductor, Inc., Suzhou* 215123, *China*
[3] *State Key Discipline Laboratory of Radio Frequency Heterogeneous Interation, Shanghai Jiao Tong University, Shanghai* 200240, *China*

(Received 13 April 2023; revised manuscript received 4 May 2023; accepted manuscript online 25 May 2023)

This paper reports a low-damage interface treatment process for AlN/GaN high electron mobility transistor (HEMT) and demonstrates the excellent power characteristics of radio-frequency (RF) enhancementmode (E-mode) AlN/GaN HEMT. An RF E-mode device with 2.9-nm-thick AlN barrier layer fabricated by remote plasma oxidation (RPO) treatment at 300 °C. The device with a gate length of 0.12-μm has a threshold voltage (V_{th}) of 0.5 V, a maximum saturation current of 1.16 A/mm, a high I_{on}/I_{off} ratio of 1×10^8, and a 440-mS/mm peak transconductance. During continuous wave (CW) power testing, the device demonstrates that at 3.6 GHz, a power added efficiency is 61.9% and a power density is 1.38 W/mm, and at 30 GHz, a power added efficiency is 41.6% and a power density is 0.85 W/mm. Furthermore, the RPO treatment improves the mobility of RF E-mode AlN/GaN HEMT. All results show that the RPO processing method has good applicability to scaling ultrathin barrier E-mode AlN/GaN HEMT for 5G compliable frequency ranging from sub-6 GHz to Ka-band.

Keywords: GaN, low damage, enhancement mode, power-added efficiency

PACS: 73.61.Ey, 73.40.Qv, 81.65.Mq **DOI:** 10.1088/1674-1056/acd8a5

1. Introduction

With the development of high-voltage switches and high-speed radio-frequency (RF) circuits, GaN semiconductors have been widely used in the field of RF power electronic devices due to their excellent material properties. The high-electron-mobility transistors (HEMTs) fabricated by conventional process are all depletion-mode devices and cannot form logic complementation. Therefore, a negative voltage circuit needs to be designed to turn off the device in circuit design.[1,2] In order to expand the application scope of GaN-based HEMT devices in mobile terminals, research on enhancement-mode (E-mode) GaN-based HEMTs has gradually become a research hotspot. Compared with the current mainstream GaAs technology, GaN technology can provide high efficiency and power density.[3–5] In short, the scaling E-mode devices bring new challenges and opportunities for the fabrication of RF E-mode devices.[6–8]

In order to achieve low-power logic complementarity, simplify the circuit structure and reduce the chip size, the conventional E-mode device fabrication process of recessed gate structure and p-GaN structure cannot ensure the fabrication of low-damage RF E-mode devices.[9–11] This is due to the scaled gate length and lateral dimensions making process compatibility problematic.[12–14] Owing to the necessity of high frequency and RF power performance, thin barrier materials with strong polarization are more conducive to fabricating RF E-mode devices. As reported, the AlN/GaN has extremely high two-dimensional electron gas (2DEG) concentration, ultra-thin barrier layer, and a process compatible with InAlN and ScAlN.[15–17] In order to reduce the influence of etching, ion implantation, and other processing methods on the 2DEG channel, we have proposed the remote plasma oxidation (RPO) processing method to fabricate AlN/GaN enhancement mode devices with excellent results.[17]

In terms of the oxidation method, there have been many studies in the literature. For example, the RIE O plasma treatment reported in Refs. [18,19] can also obtain E-mode devices, but the parallel plate in RIE mode will increase the plasma energy and inevitably cause damage to the barrier layer. In Refs. [20,21] oxygen plasma treatment at 800-W power was reported. Oxidation treatment in the full access area is difficult to control the threshold voltage and saturation current of the device during the fabrication of RF devices.

The advantage of RPO treatment is that the threshold voltage can be regulated without affecting the 2DEG channel, so that the device can be enhanced. A series of methods to enhance the device such as recessed gate and F ion implantation will cause some damage to the channel. With the positive drift of the threshold, these damages will gradually in-

†Corresponding author. E-mail: jjzhu@mail.xidian.edu.cn
‡Corresponding author. E-mail: xhma@xidian.edu.cn

© 2023 Chinese Physical Society and IOP Publishing Ltd

crease, bringing more reliability problems to the device. In the metal–insulator–semiconductor (MIS) devices, the interface between the insulating layer and the barrier layer can create problems such as heightened off-state leakage or diminished peak transconductance. Through comprehensive consideration, combining the characteristic of the AlN barrier layer oxidized easily, the RPO method is used to make the lower part of the gate into AlON that can theoretically reduce leakage, increase breakdown, and well control interface damage compared with etching. Almost no impurity particles are generated, which greatly reduces the scattering effect of impurities or defects on the 2DEG of the channel. The RPO technology also has unique advantages in making RF E-mode devices. Comparing with the conventional scaling gate and recessed gate device fabrication, the aspect ratio will cause the etching rate to drop sharply, the unstable etching rate will lead to a low yield, and the inevitable lateral etching will reduce the fidelity of the lines. The RPO approach ignores aspect ratio and enables small lines with higher fidelity, which is critical for RF device fabrication.

This paper reports the RF E-mode AlN/GaN HEMTs fabricated by the RPO treatment, with a contact resistance of 0.29 Ω·mm, a threshold voltage (V_{th}) of 0.5 V, a maximum current of 1.16 A/mm, and a 46-V breakdown voltage. It has a power density of 1.38 W/mm (0.85 W/mm) and a power added efficiency of 61.9% (41.6%) at 3.6 GHz (30 GHz).

2. Device fabrication

In this work, we used a 3-inch-thick (inch = 2.54 cm) SiC substrate epitaxial wafer fabricated by metal-organic chemical vapor deposition. From bottom to the top, the structure materials were SiC substrate, 80-nm AlN nucleation layer, 2-μm-thick UID-GaN, 2.9-nm-thick ultra-thin AlN barrier, and 2.1-nm-thick *in-situ* SiN. Hall measurement results showed that the carrier concentration at room temperature is 1.09×10^{13} cm^{-2}, the mobility is 789 cm^2/V·s, and the sheet resistance is 737.4 Ω/sq. The ohmic contact between the source electrode and drain electrode was Ti/Al/Ni/Au=20/160/55/45 nm from bottom to top, and an ohmic contact resistance formed after rapid thermal annealing at 860 °C in N_2 for 60 s was 0.29 Ω·mm. The passivation layer was grown by plasma-enhanced chemical vapor deposition of 60-nm-thick SiN, and then the sheet resistance was reduced to 320 Ω/sq. The *in-situ* SiN and PECVD-SiN under the gate were removed with CF_4/O_2 mixed plasma etching by inductively coupled plasma. Afterwards, it was determined through many experiments that the AlN region under the gate was thermally oxidized at 300 °C for 2 min by RPO treatment. After that, 450-nm-thick Ni/Au=50/400-nm metal was evaporated and used as a T-shaped gate. The schematic cross-section and HAADF-SEM of E-mode AlN/GaN HEMTs are shown in Fig. 1(a).

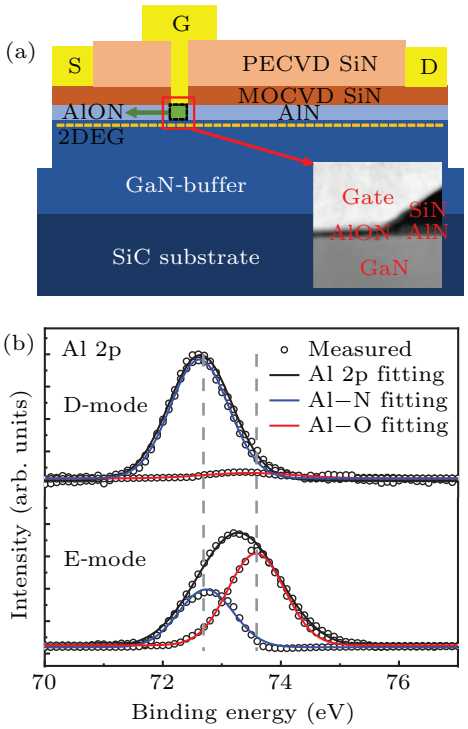


Fig. 1. (a) Schematic cross-section of device structure and high-angle annular dark field scanning electron microscope (HAADF-SEM) from E-mode AlN/GaN with RPO treatment and (b) x-ray photoelectron spectroscopy (XPS) spectra from Al 2p core levels of AlN (AlON) with and without RPO treatment.

The Al 2p core level spectra are shown in Fig. 1(b). For D-mode devices, to avoid the influence of air oxidation, Ar ions were used to etch the sample surface for 1 min before the XPS test. The Al 2p peaks consisted of two components corresponding to the Al–N bond and the Al–O bond. After the RPO treatment, the intensity of the Al–O peak was elevated, indicating that the treatment of AlN produces Al oxides on the surface. By calculating the peak area after fitting, the content of Al–O in AlON accounted for about 82.6%.

As shown in Fig. 2(a), we extracted the transfer characteristics of D-mode device and E-mode device on the same wafer with gate length $L_G = 0.12$ μm and source–drain length $L_{SD} = 1.5$ μm at $V_D = 6$ V bias. The off-state leakage of the D-mode AlN/GaN HEMT was about 2.8×10^{-7} A/mm, the saturation current was 1.74 A/mm, and the I_{on}/I_{off} ratio was 6×10^6. For the E-mode AlN/GaN HEMTs treated with RPO for 2 min, the maximum drain current was 1.16 A/mm, the off-state leakage was concentrated in the order of 7.8×10^{-9} A/mm, and a high I_{on}/I_{off} ratio was 1×10^8. However, the sub-threshold characteristics of the device were not good enough, which is caused by poor confinement of the high concentration of the two-dimensional electron gas in the AlN/GaN heterojunction. Figure 2(b) shows the transconductance curves and drain current curves of D-mode device and E-mode device in linear coordinates. The V_{th} was determined by using the linear extrapolation method. The V_{th} of D-mode and E-mode devices were −1.3 V and 0.5 V, respectively.

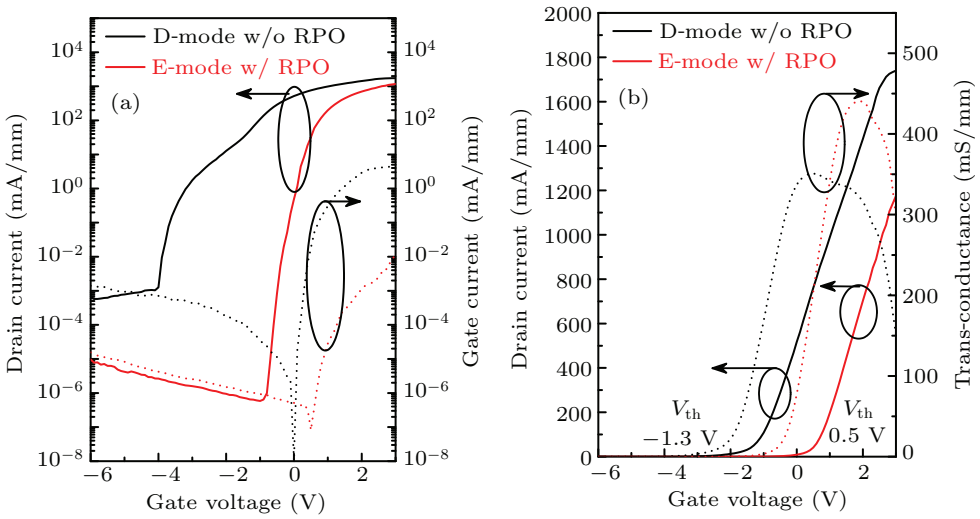


Fig. 2. Comparison of transfer characteristic between E-mode (D-mode) AlN/GaN HEMTs on (a) linear scale and (b) semi-log scale at $V_D = 6$ V.

Comparing with the D-mode device, the peak transconductance of the E-mode device increased from 351 mS/mm to 440 mS/mm. The AlN under the gate was processed by RPO to form AlON, and the concentration of 2DEG decreased, thus increasing the mobility of 2DEG. We tested the devices with $L_G = 1$ μm and $L_{SD} = 5$ μm. After the RPO treatment, the transconductance of the device increased from 175 mS/mm to 192 mS/mm. The test directly obtained the extrinsic transconductance ($g_{ext,peak}$) of the device, which are related to the intrinsic transconductance value ($g_{int,peak}$) and the device source resistance R_s, and expressed as

$$g_{ext,peak} = \frac{g_{int,peak}}{1 + g_{int,peak} R_s}. \tag{1}$$

By testing the electrical characteristics of the device in the linear region, the R_s was 3.38 Ω·mm for the D-mode device and 3.02 Ω·mm for the E-mode device. The $g_{int,peak}$ values of the two devices were calculated to be 457 mS/mm and 442 mS/mm, respectively. The RPO treatment increased the intrinsic transconductance by about 7%. The intrinsic peak transconductance of GaN-based HEMT devices could be expressed as the product of electron saturation drift velocity and gate capacitance C_g, and expressed as

$$g_{int,peak} = v_{sat} C_g, \tag{2}$$

where v_{sat} is the channel electron saturation drift velocity, and the gate capacitance takes the value when the gate voltage is 0 V. Substituting the intrinsic transconductance value and gate capacitance into Eq. (2), the channel electron saturation drift velocity v_{sat} could be obtained. The AlN gate insulating layer increased the saturation drift velocity of channel carriers from 1.11×10^7 cm/s to more than 2.04×10^7 cm/s. Therefore, the peak transconductance of the E-mode device was higher than the D-mode device.

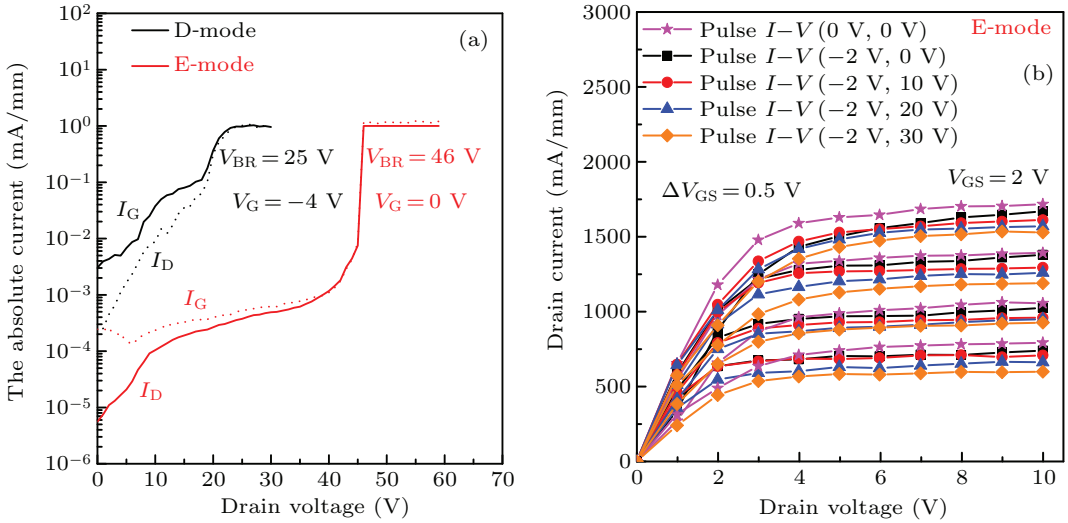


Fig. 3. (a) Three terminal off-state breakdown characteristics with D-mode and E-mode AlN/GaN HEMTs. (b) Pulsed I–V characteristics of E-mode AlN/GaN HEMTs at $V_{GS} = 0.5/1/1.5/2$ V tested under various quiescent bias conditions.

The breakdown characteristics of the devices with a source–drain spacing of 1.5 μm are shown in Fig. 3(a). The breakdown voltage was defined where the I_D reaches 1 mA/mm. The breakdown voltage increased from 25 V at $V_G = -4$ V (D-mode) to 46 V at $V_G = 0$ V (E-mode). Owing to the ultra-thin AlN barrier material, the breakdown mechanism of D-mode devices was gate-breakdown. After several tests, the breakdown mechanism of the E-mode device was transformed into source–drain breakdown, which is because the RPO treatment converts AlN under the gate into AlON, which reduces the gate leakage, and reduces the electric field strength between gate and drain.[17] The higher concentration of 2DEG formed by the AlN/GaN heterojunction led to a further increase in the electric field strength under the condition of high drain voltage. In order to obtain a higher breakdown voltage with the same source–drain spacing, we oxidized the AlN under the gate to reduce the 2DEG concentration. In this way, under the same test conditions, the electric field strength between the gate and the drain could be reduced accordingly.

As shown in Fig. 3(b), to evaluate the current collapse, the pulsed *I*–*V* characteristics of E-mode AlN/GaN HEMT at different static bias points were extracted. The pulse width and pulse period were 500 ns and 1 ms, respectively. At $V_G = 0$ V and $V_D = 0$ V and at $V_G = -2$ V, and $V_D = 30$ V, the maximum pulse current was 1.72 A/mm, 1.53 A/mm, respectively. The current collapse amount was 11%. Under the same conditions, we measured a D-mode device collapse rate of 10.9%. The interface state density can be obtained to be 4.62×10^{10} cm^{-2} (without RPO) and 8.2×10^{10} cm^{-2} (with RPO). The good interface state density proved that the RPO process has low damage to the channel.

The device used for CW power testing was a single-finger structure, $L_{SD} = 1.5$ μm, $L_G = 0.12$ μm, and $W_G = 100$ μm. As shown in Fig. 4(a), measurements were made at 3.6 GHz under CW in class AB bias conditions (quiescent drain current $I_{d,q} = 100$ mA/mm, $V_D = 10$ V, and $V_G = 0.4$ V) for RF power characterization. At the maximum efficiency (power) impedance point, the saturated output power density (P_{out}) is 1.17 W/mm (1.38 W/mm), the power added efficiency (PAE) reaches 61.9% (55.2%), and the linear gain is 14.0 dB (14.2 dB).

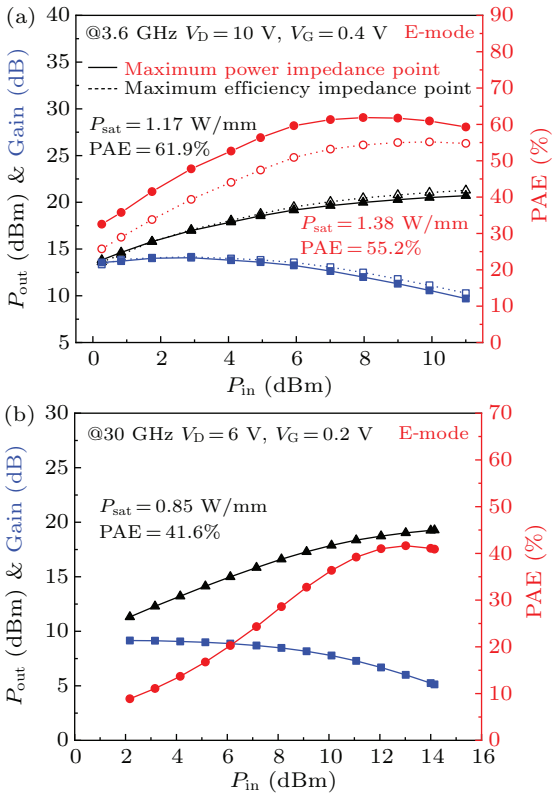


Fig. 4. CW power performance at (a) 3.6 GHz and (b) 30 GHz with E-mode AlN/GaN HEMTs with $L_{SD} = 1.5$ μm, $L_G = 0.12$ μm, and $W_G = 100$ μm, single-finger structure.

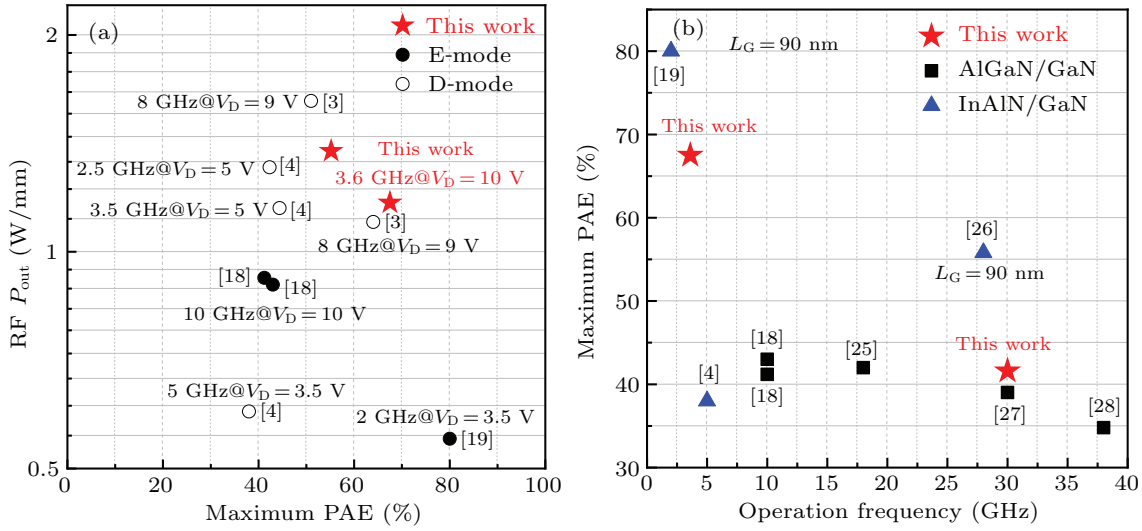


Fig. 5. (a) Benchmark of RF P_{out} as a function of maximum PAE with D/E-mode GaN-based HEMTs. (b) Benchmark of PAE versus operation frequency with GaN-based E-mode HEMTs RF power performance, including some data cited from other references.

Figure 4(b) shows that measurements that were taken at 30 GHz under CW in class AB bias conditions (quiescent drain current $I_{d,q} = 100$ mA/mm, $V_D = 6$ V, and $V_G = 0.2$ V). The results showa P_{out} of 0.85 W/mm, a PAE of 41.6%, and a linear gain of 9.15 dB. These findings indicate the enormous potential of RPO technology in the fabrication of AlN/GaN enhancement-mode RF devices. This demonstrates the great potential of RPO technology in the fabrication of AlN/GaN enhancement-mode RF devices.

As shown in Fig. 5(a), the horizontal axis is the maximum PAE of the enhancement mode device, and the vertical axis is the maximum saturated output power. We compared the power levels of D/E-mode devices for AlGaN system with those for InAlN system under low voltage. The E-mode HEMTs with strong-polarization and ultrathin barrier AlN/GaN heterostructures demonstrate that their PAEs are comparable to those with the D-mode AlGaN/GaN (InAlN/GaN) HEMTs for the RF applications. Figure 5(b) shows that the E-mode AlN/GaN HEMTs demonstrate excellent performance for Ka-band. This fully proves the practicability of RPO treatment in the AlN/GaN system for 5G-compatible frequency, mobile phone, and base station.

3. Conclusions and perspectives

This paper describes the RF E-mode AlN/GaN HEMTs fabricated by RPO treatment. The device has a V_{th} of 0.5 V, a saturation current of 1.16 A/mm, a 61.9% (41.6%) PAE, and a power density of 1.38 W/mm (0.85 W/mm) in CW power testing at 3.6 GHz (30 GHz). It is worth mentioning that the RPO treatment improves the mobility of the device while reducing the 2DEG density. All results show that the RPO processing method has good applicability for scaling ultrathin barrier E-mode AlN/GaN HEMTs for 5G compliable frequency ranging from sub-6 GHz to Ka-band.

Acknowledgements

Project supported by the Fundamental Research Funds for the National Key Research and Development Program, China (Grant No. 2020YFB1807403) and the National Natural Science Foundation of China (Grant Nos. 62174125, 62188102, and 62131014).

References

[1] Kong Y, Zhou J, Kong C, *et al*. 2014 *IEEE Electron Dev. Lett.* **35** 336
[2] Maroldt S, Haupt C, Pletschen W, *et al*. 2009 *Jpn. J. Appl. Phys.* **48** 04C083
[3] Zhou Y, Zhu J, Mi M, *et al*. 2021 *IEEE J. Electron Dev.* **9** 756
[4] Xie H, Liu Z, Hu W, *et al*. 2021 *IMWS-AMP.* **2** 397
[5] Xie H, Liu Z, Hu W, *et al*. 2020 *IEEE Microw. Wirel. Co.* **31** 141
[6] Fujii K and Morkner H 2003 *IEEE MTT-S Int. Microw. Symp. Dig.* **2** 859
[7] Feng Z H, Zhou R, Xie S Y, *et al*. 2010 *IEEE Electron Dev. Lett.* **31** 1386
[8] Huang S, Liu X, Zhang J, *et al*. 2015 *IEEE Electron Dev. Lett.* **36** 754
[9] Kong Y, Zhou J and Kong C 2014 *IEEE Electron Dev. Lett.* **35** 336
[10] Zhou Q, Chen W, Liu S, *et al.* 2013 *25th International Symposium on Power Semiconductor Devices & IC's (ISPSD)*, Kanazawa, Japan, 2013, pp. 195–198
[11] Anderson T J, Koehler A D, Greenlee J D, *et al*. 2014 *IEEE Electron Dev. Lett.* **35** 826
[12] Guerra D, Akis R, Marino F A, *et al*. 2010 *IEEE Electron Dev. Lett.* **31** 1217
[13] Radjenovic B M, Radmilovic-Radjenovic M D and Petrovic Z L 2008 *IEEE T Plasma Sci.* **36** 874
[14] Denninghoff D J, Dasgupta S, Lu J, *et al*. 2012 *IEEE Electron Dev. Lett.* **33** 785
[15] Wang R, Saunier P, Xing X, *et al*. 2010 *IEEE Electron Dev. Lett.* **31** 1383
[16] Xiao M, Duan X, Zhang J, *et al*. 2018 *IEEE Electron Dev. Lett.* **39** 719
[17] Liu S, Zhu J, Guo J, *et al*. 2022 *IEEE Electron Dev. Lett.* **43** 1621
[18] Chang C Y, Pearton S J, Lo C F, *et al*. 2009 *Appl. Phys. Lett.* **94** 263505
[19] Chang C Y, Lo C F, Ren F, *et al*. 2010 *Phys. Status. Solidi-C* **7** 2415
[20] Lee D S, Chung J W, Wang H, *et al*. 2011 *IEEE Electron Dev. Lett.* **32** 755
[21] Chung J W, Roberts J C, Piner E L, *et al*. 2008 *IEEE Electron Dev. Lett.* **29** 1196
[22] Corrion A L, Shinohara K, Regan D, *et al*. 2010 *IEEE Electron Dev. Lett.* **31** 1116
[23] Zine-eddine T, Zahra H and Zitouni M 2019 *Sci-Adv. Mater. Dev.* **4** 180
[24] Then H W, Chow L A, Dasgupta S, *et al.* 2015 *IEEE VLSI Technol.* T202
[25] Feng Z H, Zhou R, Xie S Y, *et al.* 2010 *IEEE Electron Dev. Lett.* **31** 1386
[26] Then H W, Dasgupta S, Radosavljevic M, *et al.* 2019 *IEEE IEDM*, San Francisco, CA, USA, 2019, pp. 17.3.1–17.3.4
[27] Xuan L T, Aubry R, Michel N, *et al.* 2016 *IEEE EuMIC*. 65
[28] Wang C, Chen Y C, Hsu H T, *et al*. 2021 *Materials* **14** 6558